Development of a Magnetically Coupled Mass Damper

Undergraduate Honors Thesis

Aric Scott Augustine

augustine.61@osu.edu

The Ohio State University

Department of Mechanical and Aerospace Engineering

2013

Committee:

R. Singh**,** Mechanical and Aerospace Engineering, singh.3@osu.edu

J.T. Dreyer, Mechanical and Aerospace Engineering, dreyer.24@osu.edu

B.D. Harper, Mechanical and Aerospace Engineering, harper.10@osu.edu

Presented in Partial Fulfillment of the
Requirements for Graduation with Honors Research Distinction
in the Department of Mechanical Engineering at
The Ohio State University

Table of Contents

Abstract

Tuned mass dampers can be found in a variety of rotating systems, such as automotive drivelines and motors in kitchen appliances. Such devices can suffer from low durability due to a large number of operating cycles, large displacements, and the limitations of their elastic and dissipative elements. A simplified driveline experiment is designed and used to investigate the effect of a magnetically coupled mass damper concept. The behavior of this system is examined in the time domain under a free vibration response. The addition of the magnetically coupled mass damper reduces the duration and amplitude of the vibration response of the primary system. Linear and nonlinear dynamic models are developed to explain observed coupling mechanisms (such as effective stiffness and damping elements, interfacial friction, spatial variation in magnetic loading, and drag within the bearings). A linear model is used to investigate physically tractable tuning concepts with linear parameters that are identified from measurements. The models suggest that a tuned concept could yield up to a 5 dB insertion loss in the motion of a primary system, with a slight reduction in the resonance frequency. Further work is needed to fully explore the underlying behavior.

Vita

2009.....Jackson High School, Massillon, OH

Fields of Study

Major Field: Mechanical Engineering

List of Figures

List of Tables

Chapter 1: Introduction

1.1 Background/ Literature Review

Tuned mass dampers are found in a variety of machines with rotating components, such as internal combustion engines, automotive transmissions, electric motors, and hydraulic pumps. These devices provide a means to reduce narrow-band mechanical vibrations under harmonic loading, which is common in rotating systems. A tuned mass damper can be classically modeled as a two- degree-of-freedom system, such as the one seen in Figure 1.

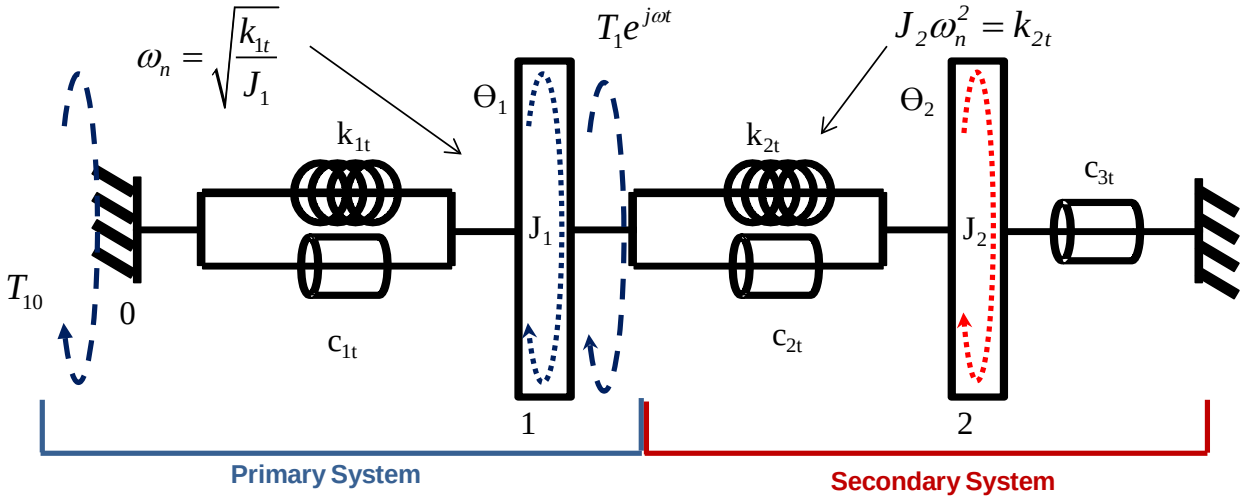

Figure 1: Analytical Representation of a Torsional System (Primary) with Tuned Mass Damper (Secondary System)

In this system, an isolated primary inertia (J_1) vibrates relative to a fixed base due to a harmonic applied torque ($T_1e^{j\omega t}$). This primary inertia has a resonance frequency ω_n that is defined by the lumped parameter mass moment of inertia (J_1) and stiffness (k_1) of the system. The variable c represents viscous damping within the system, and T_{10} represents the torque transmitted to the fixed base. Equation 1 describes the torque transmissibility between J_1 and the fixed base. Equations 2 and 3 define the variables r and ζ, respectively.

$$T_{TR} = \left| \frac{T_{10}}{T_1} \right| = \sqrt{\frac{1 + (2\zeta r)^2}{(1 + r^2)^2 + (2\zeta r)^2}} \qquad (1)$$

$$r = \frac{\omega}{\omega_n} \qquad (2)$$

$$\zeta = \frac{c_{1t}}{2\sqrt{k_{1t} J_1}} \qquad (3)$$

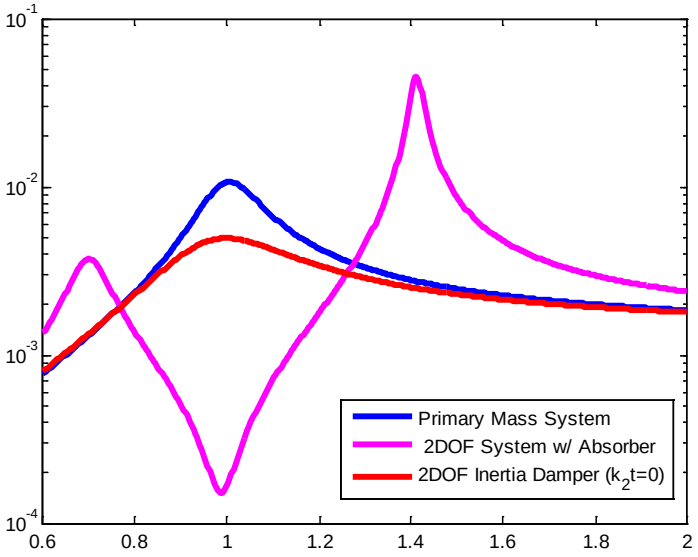

Figure 2: Behavior of Harmonic System With and Without Tuned Mass Damper

Figure 2 demonstrates the behavior of J_1 as a single-degree-of-freedom (SDOF) system under harmonic loading with damping coefficient of $\zeta \approx .07$. When J_2 and k_{12} are selected such that ω_n of the primary system is equal to that of the secondary system, then the system can be tuned so that there is very little force transmissibility at this ω_n. This is demonstrated as the "2DOF system with absorber" curve shown in Figure 2, which is the behavior of J_1 after a tuned mass damper has been added to the system. The third curve in the figure, "2DOF Inertia

Damper" shows the behavior of the system when k_2=0 and c_2 is increased, thus forming an inertia damper.

There are several examples of existing technology that make use of tuned dynamic vibration absorber or tuned mass damper theory. Dual mass flywheels (Albers 1994) and rubber shaft dampers (Stark et. al, 1999) are two examples of mechanical devices that are used as tuned dynamic vibration absorbers (first case) or tuned mass dampers (second case) to attenuate vibration. Dual mass flywheels are most commonly found in automotive applications, and are used to attenuate motion at automotive driveline resonances. They consist of two rotating inertias joined by a very long internal coil spring. Rubber shaft dampers are also widely used in the automotive industry, but can additionally be found in a variety of other rotating shaft applications. While both of these devices have been proven to be effective solutions for reducing force transmissibility at a targeted natural frequency, their main limitation is that they suffer from low durability due to the large number of operating cycles experienced, the large displacements required for many operations, and the limitation of a mechanism's elastic and/or dissipative elements.

There have also been several studies that examine the physical phenomena surrounding the vibration attenuation and force transmission capabilities of permanent magnets. For example, eddy current dampers use the relative motion of magnets to attenuate vibrations. Research shows that the magnetic coupling within these devices can be modeled as having effective stiffness and damping properties that can be used to appropriately describe the dynamic behavior of the device (Sodano et al., 2006). Magnetic gear trains have been used to demonstrate the effects of physical proximity of magnets and pole patterns on torque transmission (Atallah et al., 2004). So far, these studies have focused on torque transmission efficiency and mean load

capacity. Also, studies have been done to reduce torque variation focusing on vibration sources and acoustic radiation for brushless DC motors (Lee et al., 1995).

The common trend in all of these studies involving fixed magnetic systems is that such systems have demonstrated a limited capability for vibration attenuation. While independently inertial and magnetic vibration transmission mechanisms have limitations, a magnetic coupled mass damper could eventually combine the minimal contact benefits of permanent magnets and the inertial force coupling of standard mechanical designs.

1.2 Research Objectives

The objectives of this research are developed in order to isolate and quantify the fundamental physical phenomena that occur at the magnetic interface of a magnetically coupled mass damper concept. This is to be accomplished by designing an experimental apparatus with dynamics representative of a torsional drivetrain system. Since there are multiple dissipation mechanisms (Coulomb, viscous, structural) present in any real system, the system response both with and without the magnetic coupling must be obtained. After the response of the system is observed under a variety of conditions, a model must be developed to quantify and accurately describe the behavior of the system.

The specific goals of this project were as follows:

1) Design a simplified driveline experiment to observe the dynamic behavior of the magnetic interface.
2) Use linear and nonlinear models to explain physical phenomena observed in experiments.
3) Employ linear model to investigate tuning concepts.

By designing an experiment for which lumped parameters can be easily obtained, the assumptions made for the system can be evaluated and error within the experimental setup can be readily observed.

Chapter 2: Experiment

2.1 Single Degree of Freedom System Model

In order to study the effect of a magnetically coupled mass damper on a system, a primary system is modeled and the relevant parameters are defined. Figure 3 shows the single degree of freedom analytical model that is used to design the primary system of the experiment. As shown in this Figure, $\Theta(t)$ represents the angular displacement of a given mass moment of inertia, J_1. The constant parameters k_{1t} and c_{1t} are defined as torsional stiffness and torsional viscous damping, respectively. $T_1(t)$ represents a generic applied moment to the system.

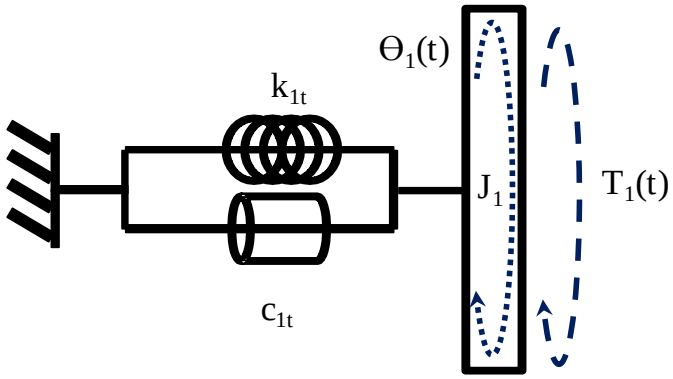

Figure 3: Single Degree of Freedom Model of Torsional System

Instead of the typical harmonic excitation conditions experienced by a traditional dynamic vibration absorber or tuned mass damper, it was decided to focus on the free response of the system when subjected to initial conditions. There are two main reasons for this input selection. First, the large translational displacement input required to produce a sufficient angular displacement makes it difficult to supply a reliable and sustainable harmonic force to the system. Second, examining the free response of the system allows for simplified identification of parameters—such as effective stiffness and damping parameters—for the SDOF and two degree of freedom (2DOF) systems in this experiment.

By selecting a free response input, $T_1(t)= 0$, resulting in the equation of motion shown in Equation 4. Equation 4 can be written in a standard form that corresponds to Equation 5 below. From this standard form, it is possible to derive relationships between the parameters of the system and values such as natural frequency (ω_{n1}) and damping ratio (ζ), which can be found in Equations 6 and 7.

$$J_1\ddot{\theta}_1(t) + c_{1t}\dot{\theta}_1(t) + k_{1t}\theta(t) = 0 \quad (4)$$

$$\ddot{\theta}_1(t) + 2\zeta\omega_{n1}\dot{\theta}_1(t) + {\omega_{n1}}^2\theta(t) = 0 \quad (5)$$

$${\omega_{n1}}^2 = \frac{k_{1t}}{J_1} \quad (6)$$

$$\zeta = \frac{c_{1t}}{2\sqrt{k_{1t}J_1}} \quad (7)$$

This model assumes that the elements of the SDOF system being modeled can be combined into discrete stiffness, damping and mass moment of inertia constants.

2.2 System Design

A simple bench-top experiment was designed in order to observe the behavior of a magnetic interface within a 2DOF system. Figure 4 shows a schematic of the proposed experimental apparatus. This system is a scaled model of a dynamic driveline system with rotational inertial components. A scaled representative system was chosen to facilitate simple modification of the system parameters, and it was also selected to isolate the fundamental physical phenomenon occurring in the magnetic coupling. A Lovejoy coupling is employed in this design in order to allow for relative motion between a fixed base and the primary inertia

while correcting for potential misalignments in the system. Springs are mounted between the two sides of the coupling to provide a means for adjusting stiffness and therefore the natural frequency of the primary system.

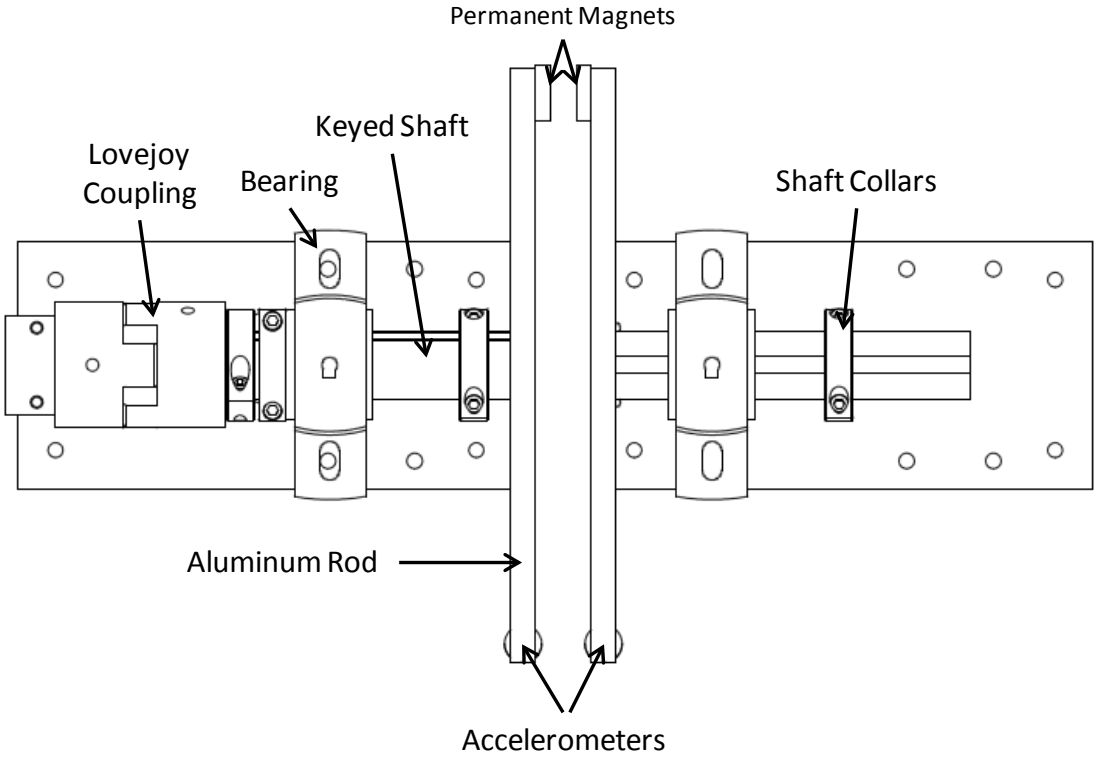

Figure 4: Schematic of the Experiment

Two 1-3/8” diameter keyed shafts are mounted on bronze self- lubricating bearings to allow for rotational motion within the system. At the end of both shafts, a stock aluminum bar is mounted. The aluminum bars serve as mounting points for the instrumentation of the experiment as well as mounting points for the permanent magnets. Shaft collars are used to add additional inertia to ensure the representative driveline dynamics of the system are achieved, and also to ensure that proper component spacing is maintained. The accelerometers used in this experiment are PCB 288D01 piezoelectric mechanical impedance sensors with a sensitivity of 100 mV/g. All measured accelerations are translational accelerations along the tangential motion direction of

the rotating bar. All results are converted to angular values to provide consistency with the models developed.

Additionally, it should be noted that the secondary mass is not constrained in the axial direction relative to its supporting bearing. Thus, when the two masses are placed close together, the attraction between the permanent magnet and its core causes the two masses to move toward one another and couple together. This attraction also caused the two shafts to become misaligned in their bearings, causing a substantial amount of additional friction in the system. To maintain adequate spacing, to reduce misalignment, and to simulate an air gap between the magnet and its core, small strips of Teflon are glued onto the face of the magnet and the core in order to prevent excessive binding of the two magnets.

Once the fundamental experimental layout is defined, various lumped parameters of the system are determined. First, the mass moment of inertia of the SDOF system is derived using solid modeling software, and is supplemented using theoretical approximations. Table 1 illustrates the relative contribution of each component in the system to the overall mass moment of inertia. The Table also displays the total effective mass of the SDOF system (J_1).

Table 1: Mass Moments of Inertia of SDOF System Components

Mass Moments of Inertia ($kg*mm^2$)	
Shaft	195
Collar	92
Coupling	490
Aluminum Bar Stock	2146
Total (J_1)	3015

In order to ensure that the primary system used in this experiment matches typical driveline resonances ($\omega_{n1} \approx$ 7-15 Hz), Equation 8 is used to select commercially available springs that would produce an appropriate natural frequency for the system.

$$k_{1t} = (\omega_{n1}^2)\, J_1 \qquad (8)$$

The first spring set selected is calculated to produce a torsional stiffness of k_{t1} = 6.2 N-m, resulting in a theoretical system natural frequency (ω_{n1}) of 7.2 Hz. The second spring set selected produces an equivalent torsional stiffness of 10.2 N-m, which gives a theoretical natural frequency of 9.3 Hz.

As mentioned when discussing the model of the SDOF system, it was decided to subject the system to an initial angular displacement ($\Theta=\Theta_0$, $(d\Theta/dt)_{t=0} = 0$). This is accomplished using a pneumatic actuator. The resting angle of the primary mass is measured first, then the actuator is activated until the desired initial position of the primary mass is achieved. To begin the dynamic experiment, the actuator is then released, allowing free vibration of the system. Figure 5 demonstrates how the system was loaded and unloaded during testing.

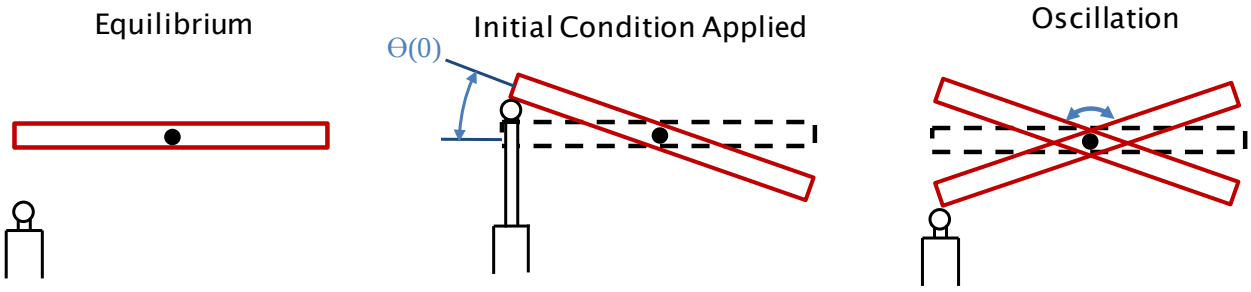

Figure 5: Actuator Position During Experimental Procedure

Based on the spring stiffness values selected, four separate test cases are chosen in order to assess the effect of stiffness, initial condition, and initial potential energy on the SDOF and 2DOF systems. These test cases are also implemented in order to determine the variability of the

system. Table 2 summarizes the test cases used. Angular displacement initial conditions are selected so that two of the cases (Case I and Case IV) have approximately the same initial potential energy. Initial potential energy is calculated using Equation 9. The initial conditions are also limited by the maximum allowable displacement of the springs in the system before they were bottomed out within the Lovejoy coupling.

Table 2: Experimental Test Cases

	k_{1t} [N*m/rad]	Θ_0*180/π [deg]	Initial Potential Energy (mJ)
Case I	6.2	5.7	30.4
Case II	6.2	7.2	49.2
Case III	10.2	2.7	11.3
Case IV	10.2	4.7	34.3

$$PE_0 = \frac{1}{2} k_{1t} \theta_0^2 \qquad (9)$$

The system is evaluated for both coupled and uncoupled responses, and each case and each coupling configuration is tested a minimum of 3 times in order to assess variability within the results. The same procedure of applying initial conditions is used for the 2DOF system. However, the primary and secondary masses are both aligned at the same angle before the actuator is released. This means that $\Theta_1(0) = \Theta_2(0)$ for each 2DOF trial conducted.

Chapter 3: Method of Procedure

3.1 Analysis of SDOF Experimental System Under Initial Conditions

In order to determine the effects of adding a magnetic coupling to the scaled torsional system, the behavior of the primary mass is first analyzed before the addition of the secondary system. Three main quantities are used to evaluate the behavior of the primary system: logarithmic decrement, maximum acceleration amplitude, and period/ frequency. These criteria are then used again to evaluate the response of the primary mass (J_1) after the introduction of the secondary mass and magnetic coupling.

Logarithmic decrement (δ) is described in Equation 10 (Rao 2011).

$$\delta = \ln\left(\frac{X_1}{X_2}\right) \quad (10)$$

This quantity expresses the ratio between two consecutive peak amplitudes of a vibratory response, X_1 and X_2. This ratio is a physical expression of the extent to which dissipative mechanisms are acting within a system. A larger δ indicates that the energy added to a system is being dissipated more quickly than a system with a smaller δ value. Equations 11 and 12 (Rao 2011) describe how logarithmic decrement (δ) is related to damping ratio and the torsional damping coefficient.

$$\zeta = \frac{1}{\sqrt{1+(2\pi/\delta)^2}} \quad (11)$$

$$c_{1t} = 2\zeta\sqrt{k_{1t}J_1} \quad (12)$$

By measuring the logarithmic decrement, it is possible to determine the median effective damping ratio of the system for each case. The results can be found in Table 3, and standard error (n=3) is also reported for each case in addition to each median value of damping ratio.

Table 3: Effective Damping Ratios for Four Cases

	k_{1t} [N*m/rad]	Θ_0*180/π [deg]	Damping Ratio [ζ]
Case I	6.2	5.7	0.15 ± 0.06
Case II	6.2	7.2	0.04 ± 0.01
Case III	10.2	2.7	0.07 ± 0.06
Case IV	10.2	4.7	0.03 ± 0.001

Equation 13 shows how standard error is reported for all collected data, where S_x is the standard deviation of the data and n is the number of samples collected.

$$e = \frac{S_x}{\sqrt{n}} \qquad (13)$$

While the damping ratio between each case varies, results show that when focusing on a single case, the damping ratio is fairly consistent when considering associated test variation. The results in Table 3 also suggest that lower damping ratios are associated with higher levels of initial potential energy applied to the system.

The second criterion used to evaluate the system is the natural frequency. Natural frequency is related to the mass moment of inertia (J_1) and stiffness (k_{1t}) within the system. Since the only changing variable related to natural frequency in the four cases is stiffness, it is expected that the theoretical and experimental natural frequencies for each case would match one another

reasonably well. Also, for cases that have the same stiffness parameter value (such as Case I and Case II), it is expected that these two cases should have approximately the same natural frequency value under a free response. Table 4 shows the median natural frequency of each case, along with the associated standard error.

Table 4: Natural Frequencies for Four Cases

	k_{1t} [N*m/rad]	Θ_0*180/π [deg]	Natural Frequency [Hz]		
			Predicted (Designed)	Measured	% Difference
Case I	6.2	5.7˚	7.19	6.76 ± 0.01	5.98 %
Case II	6.2	7.2˚	7.19	6.71 ± 0.01	6.68 %
Case III	10.2	2.7˚	9.26	9.04 ± 0.01	2.38 %
Case IV	10.2	4.7˚	9.26	9.07 ± 0.01	2.05 %

As Table 4 indicates, due to the relatively low percent difference between theoretical and experimental, all values shown are determined to be an acceptable representation of driveline dynamics. This data confirms that the proper relationship between parameters is being maintained for the SDOF system. Equation 14 describes how the percent error is defined as a comparison of predicted approximation and measured values for both natural frequency and maximum acceleration amplitude.

$$\%\ Difference = \frac{|Predicted - Measured|}{Measured} \qquad (14)$$

In order to estimate the theoretical maximum amplitude of angular acceleration for each test case, the theoretical time- domain response of a damped SDOF system to initial conditions must be examined. Equation 15 describes the theoretical angular displacement of J_1 over time

when subjected to initial conditions θ_0 and $\dot{\theta}_0$, which correspond to initial displacement and initial velocity (at time t=0) respectively (Rao 2011).

$$\theta(t) = e^{-\zeta \omega_n t}\left[\theta_0 \cos(\omega_d t) + \frac{\dot{\theta}_0 - \zeta\omega_n\theta_0}{\omega_d}\sin(\omega_d t)\right] \qquad (15)$$

In order to estimate the maximum acceleration amplitude, it is known that $\dot{\theta}_0$ =0, and it is assumed that damping is small ($\zeta \approx 0$). This leaves only the cosine portion of the time- dependent response. In addition, if damping is assumed to be negligible, then $\omega_d \approx \omega_n$. After differentiating twice, and evaluating this expression at t=0, an expression for estimating maximum angular acceleration can be expressed as shown in Equation 16. This expression serves as an upper bound for the maximum angular acceleration of the system.

$$\ddot{\theta}_{\max} \le \omega_n^2\theta_0 = \sqrt{\frac{k_{1t}}{J_1}}\theta_0 \quad (16)$$

Table 5 shows the comparison of theoretical undamped and measured maximum acceleration amplitudes.

Table 5: Maximum Acceleration Amplitude by Case

	k_{1t} [N*m/rad]	Θ_0*180/π [deg]	Maximum Acceleration Amplitude [rad/s^2]		
			Undamped Approximation (Eq. 14)	Measured	% Difference
Case I	6.2	5.7	203.6	164.2 ± 6.2	19.4 %
Case II	6.2	7.2	257.1	211.3 ± 4.6	17.8 %
Case III	10.2	2.7	159.1	157.4 ± 8.3	1.1 %
Case IV	10.2	4.7	277.5	240.7 ± 8.1	13.3 %

In all cases, the theoretical undamped maximum amplitude is higher than the measured maximum amplitude. Cases III and IV (high stiffness) have more variability than Cases I and II (low stiffness). However, the median values of maximum amplitude for the lower- stiffness cases vary from the theoretical value approximately 11% more on average. Thus, while Cases I and II are more precise, Cases III and IV are more accurate, assuming low damping.

3.2 Comparison of Uncoupled vs. Coupled Responses

Figure 6 shows a comparison of representative uncoupled and coupled response behaviors of the system. All graphs relating to the vibratory motion of the primary and secondary mass systems are shown in terms of angular acceleration (rad/s^2). Table 6 shows a comparison of logarithmic decrement (δ) and damping ratio (ζ) for all coupled and uncoupled cases. While there is a large amount of variability between these values, one noticeable trend is that apparent damping significantly increases with the addition of the secondary system; thus, the duration of the vibration response decreases.

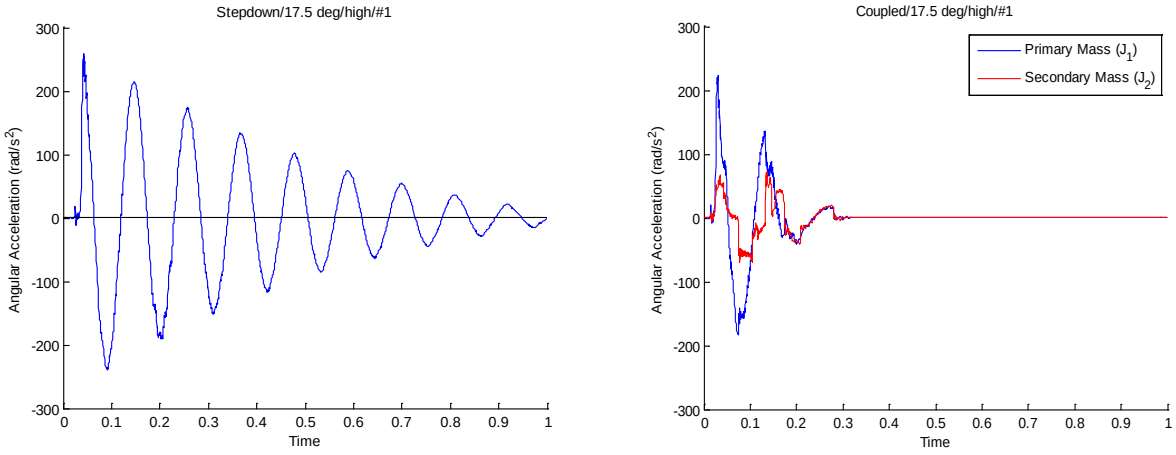

(a) (b)

Figure 6: (a) Uncoupled and (b) Coupled System Response

Table 6: Comparison of Logarithmic Decrement and Damping Ratio by Case

	k_{1t} [N*m/rad]	Θ_0*180/π [deg]	Log decrement [δ]		Damping Ratio [ζ]	
			Uncoupled	Coupled	Uncoupled	Coupled
Case I	6.2	5.7	0.95 ± 0.40	1.61 ± 0.20	0.150 ± 0.061	0.249 ± 0.028
Case II	6.2	7.2	0.26 ± 0.04	0.96 ± 0.12	0.041 ±0.006	0.151 ± 0.018
Case III	10.2	2.7	0.42 ± 0.41	1.66 ± 0.16	0.067 ± 0.062	0.256 ± 0.022
Case IV	10.2	4.7	0.20 ± 0.01	1.21 ± 0.05	0.031 ± 0.001	0.189 ± 0.007

Table 7 shows how period changed with the addition of the coupling for each of the four cases. This data shows that the 2DOF system no longer resonates at the original SDOF natural frequency. There are very few trends in this data, but for the low stiffness cases, the period decreases, while for the high-stiffness cases the period increases.

Table 7: Comparison of Damped Period by Case

	k_{1t} [N*m/rad]	Θ_0*180/π [deg]	Damped Period [ms]	
			Uncoupled	Coupled
Case I	6.2	5.7	149.6 ± 0.2	138.1 ± 3.6
Case II	6.2	7.2	149.0 ± 0.2	121.3 ± 1.5
Case III	10.2	2.7	110.8 ± 0.1	112.1 ± 5.3
Case IV	10.2	4.7	110.4 ± 0.1	116.3 ± 7.3

Table 8 shows how maximum acceleration amplitude changes with the addition of the secondary mass to the system. In all cases the maximum amplitude decreases.

Table 8: Comparison of Maximum Acceleration Amplitude by Case

	k_{1t} [N*m/rad]	Θ_0*180/π [deg]	Maximum Acceleration Amplitude [rad/s^2]	
			Uncoupled	Coupled
Case I	6.2	5.7	164.1 ± 6.2	135.7 ± 2.9
Case II	6.2	7.2	211.3 ± 4.6	177.3 ± 0.6
Case III	10.2	2.7	157.4 ± 8.3	95.9 ± 9.9
Case IV	10.2	4.7	240.7 ± 8.1	218.7 ± 6.1

3.3 Linear Model

While several characteristic quantities are measured or calculated for both the SDOF and 2DOF systems, it is difficult to establish any significant trends within the data presented in the previous section. In order to further characterize the behavior of the experiment, analytical models are developed in an attempt to explain the system behavior more precisely. Figure 7 shows a schematic of the linear 2DOF model developed for the experimental system used. The Figure also labels what components of the experimental apparatus correspond to what linear

elements in the model. For example, k_{1t} represents the torsional stiffness of the Lovejoy coupling, and c_{1t} represents the viscous damping present in the bearing supporting one of the shafts, as well as any other dissipative mechanisms within the primary mass system. In this model, it is assumed that the magnetic coupling has traditional linear stiffness and viscous damping parameters. k_{2t} and c_{2t} represent the equivalent stiffness and damping of the magnetic coupling in the system.

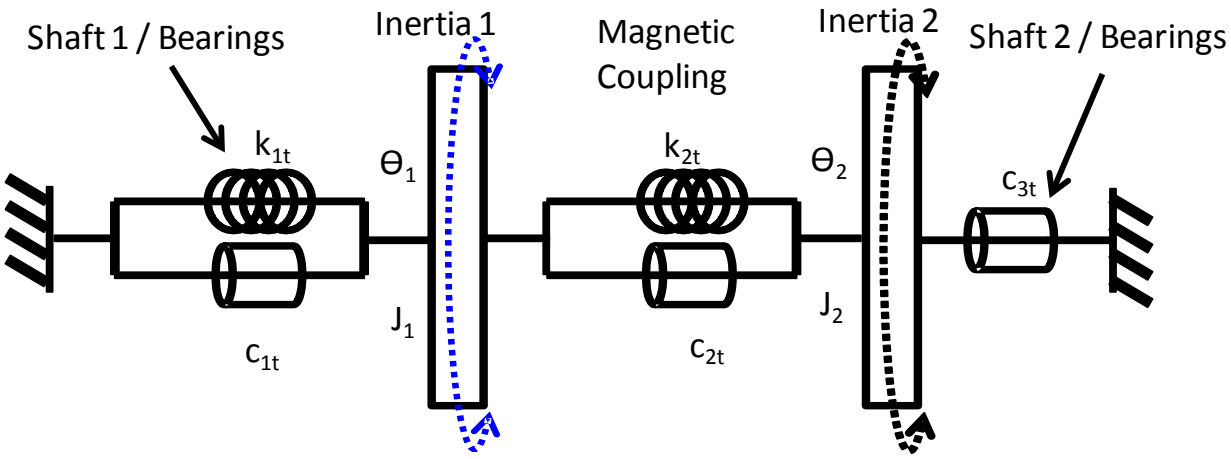

Figure 7: 2DOF Linear Model of the Torsional System with Magnetic Coupling

The equations of motion for this simple 2DOF linear model can be written in matrix form, as shown in Equation 17.

$$\begin{bmatrix} J_1 & 0 \\ 0 & J_2 \end{bmatrix}\begin{Bmatrix} \ddot{\theta}_1(t) \\ \ddot{\theta}_2(t) \end{Bmatrix}+\begin{bmatrix} (c_{1t}+c_{2t}) & -c_{2t} \\ -c_{2t} & (c_{2t}+c_{3t}) \end{bmatrix}\begin{Bmatrix} \dot{\theta}_1(t) \\ \dot{\theta}_2(t) \end{Bmatrix}+\begin{bmatrix} (k_{1t}+k_{2t}) & -k_{2t} \\ -k_{2t} & k_{2t} \end{bmatrix}\begin{Bmatrix} \theta_1(t) \\ \theta_2(t) \end{Bmatrix}=\begin{Bmatrix} 0 \\ 0 \end{Bmatrix} \qquad (17)$$

Using a combination of MATLAB ODE solvers, the system of equations shown in Equation 17 are solved and graphed. It should be noted that in order to achieve a solution for these equations, it is assumed that c_{3t} and c_{1t} are both equal to the values calculated from the logarithmic decrement of the SDOF system. For each case outlined in the previous sections, the equivalent k_{2t} and c_{2t} of the system are determined using a least squares method by comparing

the experiment and model results. Figure 8 shows a representative comparison between an (a) experimental result and (b) the corresponding linear model prediction. While the general physical trends of the model agree with those of the experimental results, the main qualitative difference between the experimental behavior and the model behavior is at the peak amplitudes of these responses.

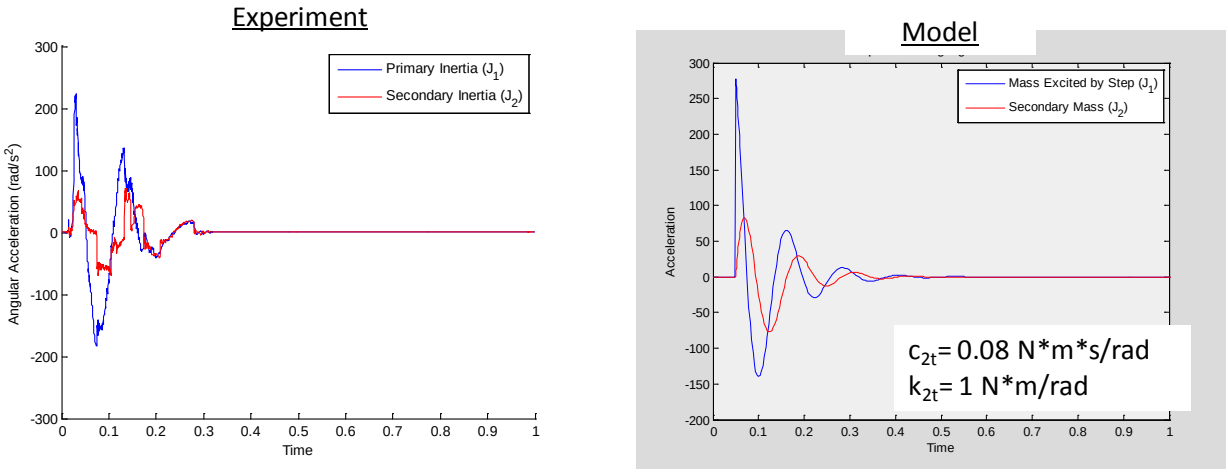

(a) (b)

Figure 8: Comparison of (a) Measurements and (b) Predictions

Table 9: Equivalent Linear k_{2t} and c_{2t} Elements for Four Cases

	k_{1t} [N*m/rad]	Θ_0*180/π [deg]	Initial PE [mJ]	c_{2t} [N*m*s/rad]	k_{2t} [N*m/rad]
Case I	6.2	5.7˚	30.4	0.1	2
Case II	6.2	7.2˚	49.2	0.08	1
Case III	10.2	2.7˚	11.3	0.12	3
Case IV	10.2	4.7˚	34.3	0.08	1

Table 9 shows the equivalent stiffness (k_{2t}) and viscous damping (c_{2t}) that were found for the magnetic coupling for each case. Two main observations are gathered from this data. First, as initial potential energy increases between the test cases, the equivalent stiffness and damping values of the magnetic coupling decrease. This suggests that as more energy is added to the system, the magnetic coupling is able to transmit less vibration. Also, if the system is truly linear, it would be expected that c_{2t} and k_{2t} would be the same value regardless of changes made to the system. However, since the values are changing between the different test cases, this suggests that the system might contain nonlinear elements.

Table 10 shows a comparison of maximum amplitude and logarithmic decrement between the linear model and the experimental results. While these results also confirm basic physical trends, such as the maximum amplitude increasing as initial potential energy increases, the large variability between experimental and model values suggest that the linear model is not the best fit for the experimental behavior.

Table 10: Experiment vs. Linear Model Amplitude and Decrement

	k_{t1} [N*m /rad]	Θ_0 [deg]	Initial Potential Energy [mJ]	Maximum Acceleration Amplitude (rad/s^2)		Logarithmic Decrement (δ)	
				Experiment	Model	Experiment	Model
Case I	6.2	5.7	30.4	135.7	199.8	1.6	1.9
Case II	6.2	7.2	49.2	177.3	252.3	1.0	1.9
Case III	10.2	2.7	11.3	95.9	155.6	1.7	1.9
Case IV	10.2	4.7	34.3	218.7	273.1	1.2	1.4

As shown previously in Figure 8, while for most instances the linear model agrees with the general physical trends of the experimental results, the experimental results do not yield the same smooth acceleration behavior as the linear model. In particular, the peak accelerations of

the experimental results exhibited a “jagged” behavior. This behavior suggests that additional physical mechanisms are present in the system that are not accounted for by the linear model.

Since Teflon strips are placed between the magnet and the core in order to provide consistent spacing between these elements, it is hypothesized that friction at this interface could also be affecting the dynamic response of the system. There are several factors taken into consideration when attempting to describe the behavior of the friction force within the magnetic coupling.

The first factor that is not accounted for in the linear model is the normal load between the magnet and its core. Because the magnet and the core experience relative motion while the experiment is running, the normal load between the two surfaces will fluctuate depending on the amount of overlap between these two components. However, this normal load is insignificant unless it is assumed that there is friction at the magnetic interface.

Friction within the system could also lead to a stick- slip phenomenon at the interface. Under stick- slip conditions, the masses become temporarily coupled together by static friction because of low relative acceleration. The masses continue to be statically coupled until the relative acceleration between the two masses is large enough to cause the friction force to transition back to kinetic friction.

Finally, it is possible that the coefficient of friction itself could be a function of relative displacement between the two masses of the system. All of these factors are considered during the development of a nonlinear system model intended to improve the understanding and approximation of the physical mechanisms within the system.

3.4 Nonlinear Model

Because the linear model does not sufficiently describe the behavior of the experiment, a model with nonlinear elements is developed. Figure 9 shows a graphical representation of this model. Several assumptions are made to develop the model.

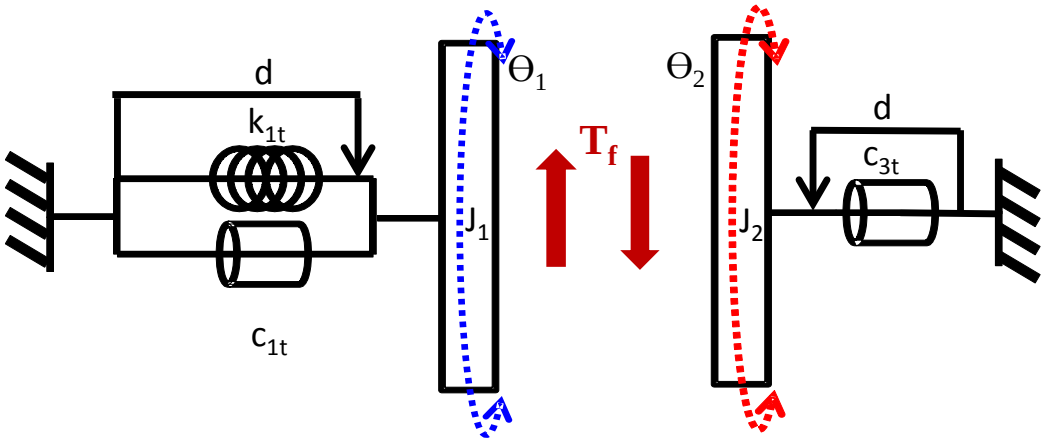

Figure 9: Nonlinear 2DOF Analytical Model

First, it is assumed that Coulomb friction is the main dissipation mechanism acting between the primary and secondary system. It is also assumed that the friction torque (T_f) is a function of magnetic overlap, which is in turn a function of the relative position of the two masses. The same constant mass moment of inertia and stiffness parameters are used for this model. A drag element is also added on either side of the model in an attempt to better describe the behavior of the self-lubricating bearings within the system. Drag is determined by conducting static and dynamic tests to determine static and dynamic friction coefficients. In order to confirm that the viscous damping elements for the nonlinear model should have the same constant value as for the linear 2DOF and SDOF models, the nonlinear model is first exercised as a SDOF free vibration response. The SDOF model response is then compared to the SDOF experimental

results. Since the behavior of the nonlinear model with both drag and linear viscous damping coefficients is consistent with the experimental behavior, no change to the viscous damping parameter for the bearings is required.

Equations 18 and 19 show the equations of motion derived for the nonlinear system.

Table 11 summarizes the parameters used in these equations.

$$J_1\ddot{\theta}_1 + c_{1t}\dot{\theta}_1 + k_{1t}\theta_1 + d\tanh(v\dot{\theta}_1) + \tanh[v(\dot{\theta}_1 - \dot{\theta}_2)]N\mu R = 0 \quad (18)$$

$$J_2\ddot{\theta}_2 + c_{1t}\dot{\theta}_1 + d\tanh(v\dot{\theta}_2) - \tanh[v(\dot{\theta}_1 - \dot{\theta}_2)]N\mu R = 0 \quad (19)$$

Table 11: Nonlinear Model Parameter Definitions

Variable	Definition	Units
R	Radius of Aluminum Rod	m
r	Radius of Magnet Face	m
μ	Dynamic Coefficient of Friction	n/a
ν	Smoothing Constant	n/a
d	Bearing Drag	N*m
N	Pull Force of Permanent Magnet	N

The normal force (N) provided by the magnet's pull force is one of the parameters that defines the friction force within the system. There are two expressions developed for the normal force. First, the normal force is expressed as a constant value. Second, the normal force is expressed as a linear function of the relative position between the two masses, and therefore the two magnets. Equation 20 shows how the normal force is defined as a linear function.

$$N = 100 - 100\left(\frac{R}{2r}\right)\left|\theta_1 - \theta_2\right| \quad (20)$$

This definition of the normal force as a function of the relative position of the two magnets is developed based on the criteria that the normal force should be at a maximum when there is complete overlap between the magnet and its core ($\Theta_1 - \Theta_2 = 0$), and that the normal force should be zero when the magnet and its core are no longer overlapping ($\Theta_1 - \Theta_2 = 2r/R$). Basic trigonometry is used to derive the position at which the magnets would no longer overlap Finally, a conditional statement is defined to ensure that the normal force could not be expressed as a negative number, since this behavior would have no physical meaning for the system defined.

Figure 10 shows a comparison between the experimental response and the nonlinear model with (a) constant and (b) linearly varying normal force. By using a similar least squares technique as with the linear model, the coefficient of friction between the two masses is altered until the model response most closely matched the experiment.

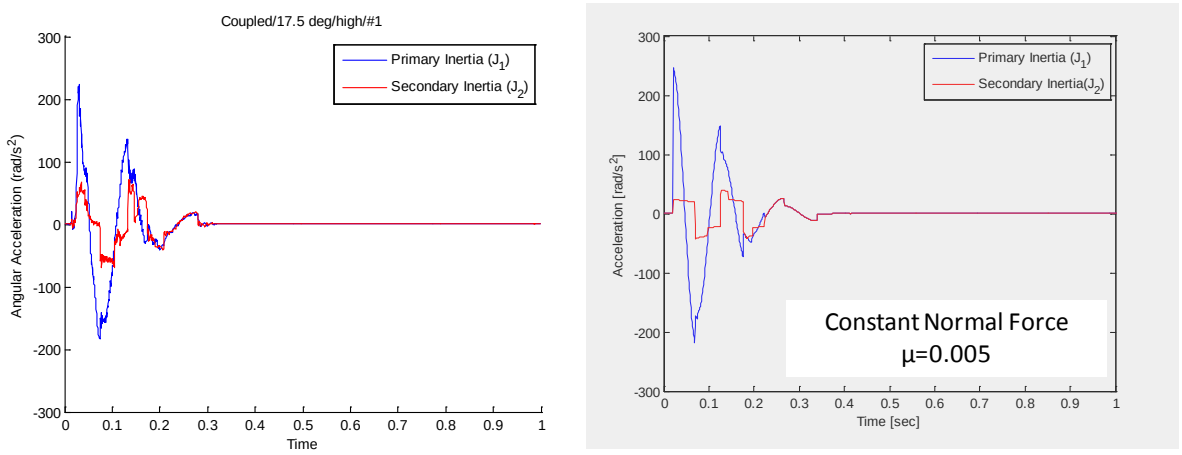

(a)

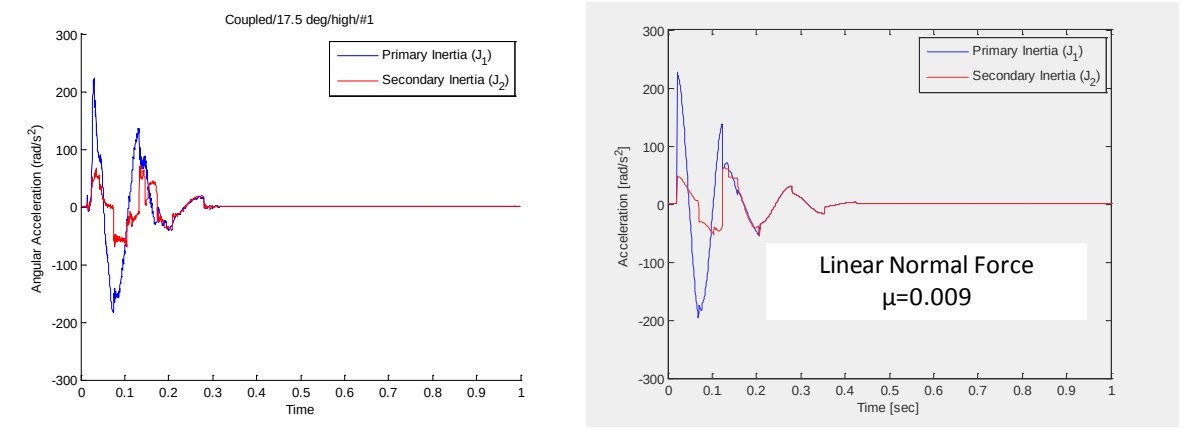

(b)

Figure 10: Experiment vs. Nonlinear Model Comparison
(a) Constant Normal Force (b) Linear Normal Force

Figure 10 demonstrates that the nonlinear model is much more effective at matching the response of the system than the linear model. By comparing the nonlinear model to the experimental results, it is possible to verify that it is necessary to include nonlinear elements in the model in order to more accurately describe the experimental system behavior. Furthermore, it can be seen in the Figure that using a linear function of relative inertia position to define the normal force between the magnet and the core provides a more accurate representation of the experimental data.

3.5 Linear Tuning Concepts

The experimental system was not initially designed as a tuned mass damper because the primary focus of this research is to study the physical phenomena surrounding the behavior of a magnetic interface within a representative driveline dynamic system. However, after verifying that the linear model is an acceptable simplified model of the behavior of the system, it is possible to exercise this model to determine the feasibility of tuning the system to maximize vibration reduction.

As outlined in Chapter 1, it is possible to tune the secondary system of this experiment by ensuring that the natural frequency of the secondary system (ω_{n2}) is equal to that of the primary system (ω_{n1}). In examining this problem, it is assumed that the parameters defining the primary system cannot change, and the design variables are only those within the secondary system. Based on this assumption, there are two options to increase ω_{n2} to the desired value based on the definition of the natural frequency of a linear system. First, the torsional stiffness of the magnetic coupling (k_{2t}) can be increased. Second, the secondary mass moment of inertia (J_2) of the system can be reduced.

Case IV (k_{t1}= 10.2 N*m/rad, Θ_0 = 4.7˚) is selected as a representative case for this study. The primary mass of the system for Case IV has a natural frequency of ω_{n1}= 9.3 Hz. However, the secondary mass has a natural frequency of ω_{n2}= 3.2 Hz. This results in a required increase of ω_{n2} by a factor of approximately 2.8. The first parameter of the secondary system that can be adjusted to cause this change is torsional stiffness. Equation 21 shows how torsional stiffness is defined for the magnetic coupling.

$$k_{2t} = k_2 R^2 \quad (21)$$

Assuming that k_2, the effective "translational" stiffness of the magnet, cannot be changed, the only variable that can be changed to increase the effective stiffness of the secondary system is R, the radius of the aluminum bar. By using the relationship in Equation 21 and the definition of natural frequency, it is determined that in order to achieve the appropriate change in $\omega_{n2,}$ the radius of the bar also must be increased by 2.8 times. Augmenting the geometry of a system by a factor of 2.8 would not be a practical design option for a real system, as it would cause packaging difficulties.

The other option for changing ω_{n2} is to decrease the mass moment of inertia of the secondary system (J_2). It is determined through the definition of natural frequency that J_2 would need to be reduced by a factor of 8 to achieve the desired response. This option is much more feasible from a design perspective, especially for an automotive design application where it is often desired to reduce weight without causing negative vibration effects.

Since reducing the secondary system moment of inertia was determined to be the most practical design option, this change is made to the linear model and the frequency response for both tuned and untuned systems is calculated. Using the equations of motion defined in Equation 17, the system of equations for the linear system in the Laplace domain are defined as shown in Equation 22. Equation 23 shows the resulting transfer function that is used to determine the frequency response of the linear system.

$$\begin{bmatrix} J_1 s^2 + (c_{2t} + c_{3t})s + k_{2t} & -(c_{2t}s + k_{2t}) \\ -(c_{2t}s + k_{2t}) & J_1 s^2 + (c_{2t} + c_{3t})s + k_{2t} \end{bmatrix} \begin{Bmatrix} \Theta_1(s) \\ \Theta_2(s) \end{Bmatrix} = \begin{Bmatrix} F_0 \\ 0 \end{Bmatrix} \qquad (22)$$

$$\frac{\Theta_1}{F_0}(s) = \frac{J_2 s^2 + (c_{2t} + c_{3t})s + k_{2t}}{[J_1 s^2 + (c_{1t} + c_{2t})s + k_{1t} + k_{2t}][J_2 s^2 + (c_{2t} + c_{3t})s + k_{2t}] - (c_{2t}s + k_{2t})^2} \qquad (23)$$

Figure 11 shows a comparison of the accelerance frequency response function for (a) an untuned and (b) a tuned response. A significant reduction in resonance amplitude is achieved after tuning the system, resulting in an increase in insertion loss from 1 dB to 5 dB. It should also be noted that the resonance frequency is shifted slightly when tuned, from 9.0 Hz to 8.6 Hz. Equation 24 shows how insertion loss for both tuned and untuned cases was calculated, where A represents accelerance (α/T_1).

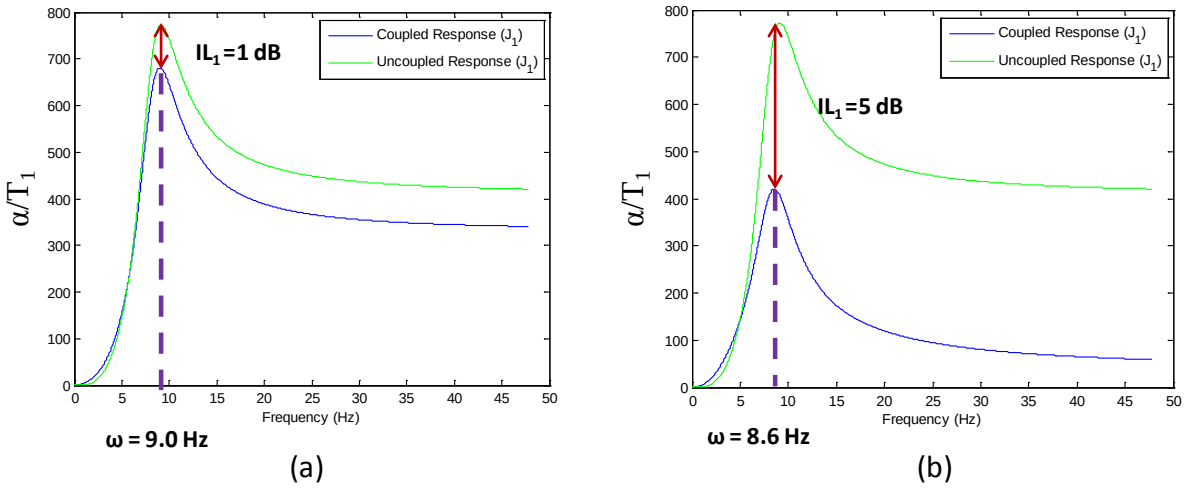

Figure 11: Insertion Loss and Resonance Shift for (a) Untuned and (b) Tuned Response

$$IL = 20\log\left(\frac{A_{\text{without absorber}}}{A_{\text{with absorber}}}\right) \qquad (24)$$

3.6 Frequency Response Discussion

After examining Figure 11, it can be seen that the predicted frequency response of the linear model is different from the one predicted in Chapter 1, Figure 2. The response shown in Figure 2 describes the expected response of the primary system if the primary and secondary inertias were coupled by both a stiffness and damping element. For this 2DOF system, there are two resonance peaks. However, only one resonance peak is predicted using the linear model and the experimentally determined parameters for Case IV. This suggests that the dissipative effects of friction within the magnetic interface are much larger than the restorative force between the magnet and its core.

Figure 12 shows the frequency response of the linear model under various conditions. The uncoupled model has one resonant frequency as expected. However, the 2DOF system continues to have one resonance peak using the parameters for k_{2t} and c_{2t} determined from the experiments. However, when damping is ignored within the coupling, we see that two resonance peaks once again appear, suggesting that the tuned system is heavily damped (by rough calculations based on J_2, k_{2t}, c_{2t} and c_{3t} , $\zeta > 0.5$). When the effective stiffness of the coupling (k_{2t}) is set equal to zero, the response is approximately the same, and only the resonance amplitude is noticeably changed, suggesting that the interfacial stiffness still plays a significant role in the system response and should not be ignored. Table 12 summarizes the resonance frequency and maximum accelerance of each model configuration shown in Figure 12.

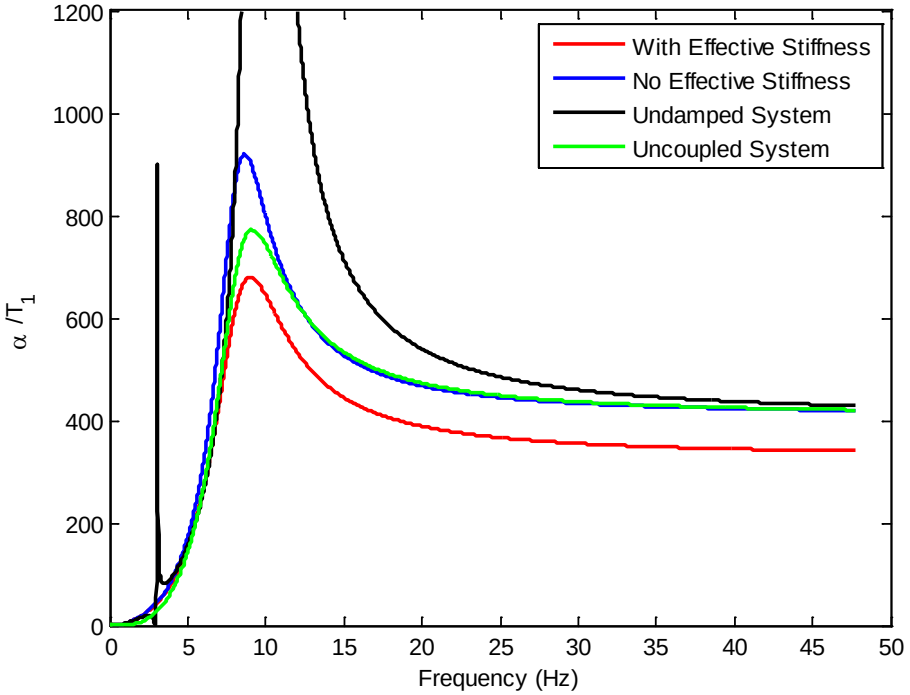

Figure 12: J_1 Frequency Response from Linear Model for System with Effective Stiffness, No Effective Stiffness, Undamped System, and Uncoupled System

Table 12: Resonance Frequency and Maximum Accelerance of Effective Stiffness, No Effective Stiffness, Uncoupled, and Undamped Cases

	Resonance Frequency (Hz)	Maximum Accelerance $(kg*m^2)^{-1}$
With Effective Stiffness (k_{2t})	9.0	680.7
No Effective Stiffness (k_{2t}=0)	9.0	873.9
Undamped System ($c_{2t,}$=0)	3.1 / 9.8	900.1 / 7069.2
Uncoupled System ($k_{2t,}c_{2t}$=0)	9.2	772.1

Figure 13 shows the free transient response modeled for each case outlined above. This comparison shows that a secondary system with no damping does not attenuate the amplitude of the vibrations, but does cause a phase shift in the free response corresponding to a change in natural frequency. When damping in the magnetic coupling is added, the amplitude and duration

of the oscillations decreases substantially, and the behavior of the system more closely matches experimental results. The two damped cases plotted with and without effective interfacial stiffness are very similar in behavior. This suggests that the system could be considered as an inertial damper. Further physical evaluation of the system under harmonic conditions is required to better understand the significance of the interfacial stiffness.

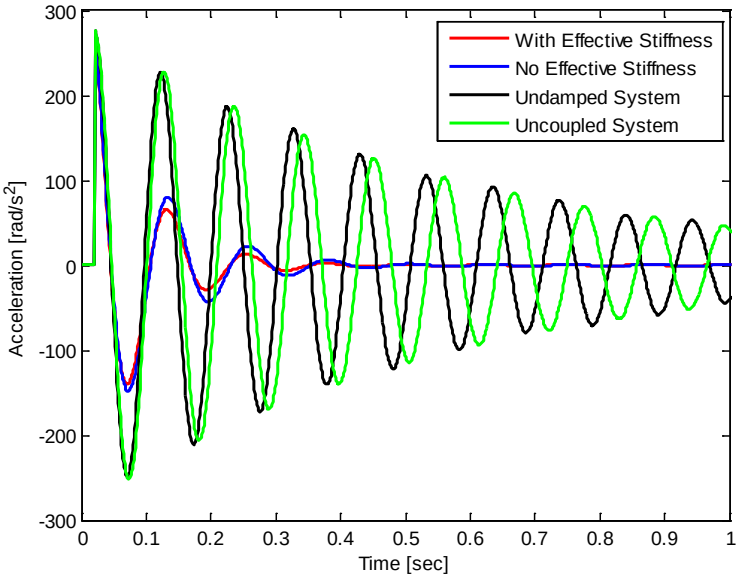

Figure 13: Frequency Response from Linear Model for System with Effective Stiffness, No Effective Stiffness, Undamped System, and Uncoupled System

Chapter 4: Conclusion

4.1 Sources of Error

The objective of this experiment is to develop models of a system and gain insight into its physics; therefore, an exact match of theory with experiment is not necessary. A significant portion of the variability in this research is believed to have come from the experimental apparatus. Misalignment of the various components within the system is a major concern during the data collection. The magnets are only mounted on one side of the mass, causing axial deviation of the shafts, which could in turn caused unpredictable changes in perceived effective damping within the system.

The Lovejoy coupling used in the system also provides for some variability within the measurements. The alignment of the springs and the change in stiffness associated with the shifting of the springs during experimental trials could have also contributed to some error within the system. In order to best mitigate the effects of this, any time the primary system springs are changed, both uncoupled and coupled responses are measured to allow for a more direct comparison. In addition, the maximum deflection of the springs is also taken into account, and only initial conditions that ensured the springs would not “bottom out” during testing are chosen.

4.2 Summary

A simplified driveline experiment is designed and built in order to study the effect of a magnetically coupled mass damper concept. The system is designed to have two degrees of freedom, a primary system and a secondary system, representing the tuned mass damper. The setup is also designed to adjust the primary system stiffness, thereby changing the primary

system resonance. The parameters of the system are determined by examining the free response of the primary experimental system under initial conditions. The addition of the magnetically coupled mass damper reduces the duration and amplitude of the vibration response of the primary system.

Both linear and nonlinear models are developed to attempt to describe the system behavior to investigate the physical mechanisms within the system and better understand the observed experimental behavior. The linear model of the system uses a least squares method to determine the approximate effective stiffness and damping of the magnetic coupling within the system. The linear model captures relative trends in terms of duration and maximum amplitude for the different cases. A nonlinear model is derived to gain more insight into the coupling mechanisms associated with the magnetic interface, such as friction, spatial variation of the magnet normal load, and drag within the bearings.

While the linear model does not capture all of the behavior within the experimental system, it is able to describe some of the general physical trends. For this reason, the model is used to examine potential tuning concepts with identified linear parameters from the experimental study. Using linear tuning concepts, it is shown that it is possible to reduce the resonant amplitude of the system (1dB to 5dB insertion loss) while the observed resonance of the system is also slightly shifted and reduced.

4.3 Recommendations for Future Work

While a lot of useful information is gathered as a result of this research, there are still several opportunities for future investigation. First, since the linear model is used to identify the theoretical response of the experimental setup due to a harmonic excitation, it would be of

interest to validate the predicted behavior by finding a controlled manner to apply harmonic excitation to the system.

The effect on the system regarding the type of magnet used would also be a good topic of continued exploration for this project. Magnet polarization profiles, magnet size, and magnet geometry would most likely play an important factor in the force transmissibility capabilities of a magnetic coupling. These considerations could also lead into an investigation of packaging concerns for a magnetically coupled mass damper device.

The relative motion of magnets at the high frequencies or amplitudes associated with driveline dynamics would also cause the temperature of the magnets to be a concern. If the relative motion of the primary and secondary system caused the temperature of the magnets to increase, their effectiveness to attenuate vibrations could diminish.

Finally, while this experiment only examines the response of a system with one magnet-core pair, looking at the spatial effects of multiple magnets on each side of the system would also improve understanding of the fundamental physical phenomena present within magnetic couplings as related to tuned mass dampers.

This study is specific to the hardware and system studied. Further work is needed to fully explore the underlying behavior of this system and how to understand issues for broader applications of the proposed concepts.

REFERENCES

Albers, A. “Advanced Development of Dual Mass Flywheel (DMFW) Design- Noise Control for Today’s Automobiles.” 5th LuK Symposium (1994).

Atallah, K., S.D. Calverley, and D. Howe. “High- Performance Magnetic Gears.” Journal of Magnetism and Magnetic Materials 272–276 (2004) e1727–e1729.

Hartog, J. P. Den. Mechanical Vibrations. New York: Dover Publications, 1985.

Lee, M.R., C. Padmanabhan and R. Singh. “Dynamic Analysis of a Brushless D.C. Motor by Using a Modified Harmonic Balance Method.” Journal of Dynamic Systems,Measurement and Control 117(3), 283-291 (1995).

MATLAB. Vers. R2009a. Natick, MA: The Math Works, Inc., 2009. Computer software.

Rao, S.S. Mechanical Vibrations. Upper Saddle River, NJ: Prentice Hall, 2011.

Sodano, H.A., J. Bae, D.J. Inman, and W. Keith Belvin. "Improved Concept and Model of Eddy Current Damper." Journal of Vibration and Acoustics 128.3 (2006): 294.

Stark, M.H. and G.A. Conger. Drive Shaft Damper. Arrow Paper Products, Co, assignee. US Patent 5976021. 2 Nov. 1999.

Appendix A: List of Symbols and Abbreviations

$A_{with\ absorber}$	Resonant Accelerance Amplitude With Absorber [rad/s^2]
$A_{without\ absorber}$	Resonant Accelerance Amplitude Without Absorber [rad/s^2]
c_t	Torsional Viscous Damping [N*m*s/rad]
d	Drag Torque [N*m]
e	Standard Error [ ]
IL	Insertion Loss [dB]
J	Mass Moment of Inertia [kg*m^2]
k	Linear Stiffness [N/m]
k_t	Torsional Stiffness [N*m/rad]
n	Number of Samples [ ]
N	Magnet Normal Force [N]
PE_0	Initial Potential Energy [mJ]
r	Frequency Ratio [ ]
R	Radius of Aluminum Bar [m]
r	Radius of Magnet [m]
S_x	Standard Deviation of Samples [ ]
T	Torque [N*m]
t	Time [s]
T_f	Friction Torque [N*m]
X_1	First Acceleration Peak Amplitude [rad/s^2]
X_2	Consecutive Acceleration Peak Amplitude [rad/s^2]

δ	Logarithmic Decrement [ ]
ζ	Damping Ratio [ ]
Θ_0	Initial Angular Displacement [rad]
Θ_1	Primary System Angular Displacement [rad]
Θ_2	Secondary System Angular Displacement [rad]
μ	Coefficient of Friction [ ]
ν	Smoothing Coefficient [ ]
ω	Forcing Frequency [Hz]
ω_{n1}	Primary System Natural Frequency [Hz]
ω_{n2}	Secondary System Natural Frequency [Hz]